3. Solution Structure of [Me-L-Leu^7]Didemnin B Determined by NMR Spectroscopy and Refined by MD Calculation

by **Horst Kessler*** and **Siggi Mronga**

Organisch-Chemisches Institut, TU-München, Lichtenbergstr. 4, D–8046 Garching

and **Martin Will**

BASF, D–6700 Ludwigshafen

and **Ulrich Schmidt**

Organisch-Chemisches Institut, Biochemie und Isotopenforschung der Universität, Pfaffenwaldring 55, D–7000 Stuttgart

(4.X.89)

Several homo- and heteronuclear two-dimensional NMR techniques were used to assign all H- and C-resonances of the two conformers **A** and **B** of [7-(*N*-methyl-L-leucine)]didemnin B. Didemnine is a biologically highly active cytostaticum and immunosuppressivum. The assignment of the aliphatic C-atoms were done by the inverse H,C-COSY with TOCSY transfer which connects complete proton spin systems and represents them on C-atoms. The structure of both conformers (**A** and **B**) in (D_6)DMSO solution was derived from homo- and heteronuclear couplings (*J*), temperature dependencies of NH protons, and NOE effects. Distances determined from the latter were used for refinements by restrained MD calculations using the GROMOS program. The solution structure of [Me-L-Leu^7]didemnin B (**A** and **B**) was compared to that of didemnin B. The backbone structure of the macrocyclic ring and of the linear side-chain moiety are very similar in conformer **A** and didemnin **B**, though the Ist^1-Hip^2 region of the ring is slightly extended in conformer **A**. This may be caused by the influence of the Me-L-Leu^7 residue in **A** and may be responsible for its reduced biological activity in comparison to didemnin **B**. The more weakly populated conformer **B** exhibits a βVI turn in the linear side-chain moiety.

Introduction. – Didemnin B is a new highly potent cytostaticum [1]. It belongs to a family of cyclic depsipeptides isolated from a caribbean tunicate of the family Didemnidae *(Tridemnum genus)*. Recently, the synthesis of didemnins was reported by different groups [2–4]. The conformation of didemnin A and B was determined by NMR spectroscopy [5] [6] and computer calculations [6], and compared to the structure of didemnin B in the crystal, obtained by an X-ray analysis [7].

The interesting pharmacological properties stimulated us to synthesize derivatives and correlate their structure and activity. Here we report the structure of a derivative with an *N*-methyl-L-leucine (Me-L-Leu; short form, MeLeu) residue instead of a Me-D-Leu in position 7 *(Fig. 1)*. Its 500-MHz ^{1}H-NMR spectrum exhibits a fourfold signal set which could result from rotamers about one or several of the secondary amide bonds and/or partial racemization during synthesis. The sample was pure in HPLC indicating that inversion of configuration of an amino acid in the depsipeptide ring can be excluded. Indeed, in such a case we would expect a drastic change in the conformation of the ring, giving rise to a strongly changed HPLC retention time as well as a strong differentiation of the NMR parameters of almost all amino acids in the ring. This was not observed. A

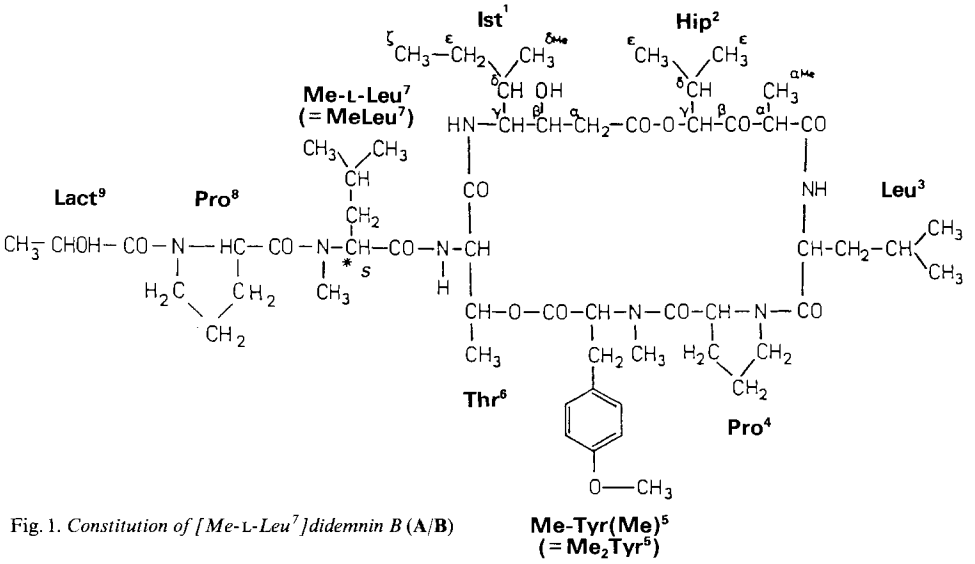

Fig. 1. *Constitution of [Me-L-Leu⁷]didemnin B* (**A**/**B**)

racemization at the most sensitive part, at the MeLeu⁷ residue, could be excluded by comparing the spectrum with that of didemnin B which contains Me-D-Leu⁷.

Hence, the evaluation of the spectra were initially performed on the assumption that all four isomers (ratio of 57.0:24.4:15.1:3.5), which we call **A**, **B**, **C**, and **D**, are conformational isomers. It turned out later that exchange occurs only between **A** and **B** as well as between **C** and **D**. This observation stimulated the synthesis of an additional epimer containing the D-lactoyl moiety (D-Lact) instead of L-Lact⁹, as partial racemization was the remaining possibility for the explanation of the occurrence of four signal sets. In fact, **C** and **D** could be identified as the D-Lact⁹ epimer of [Me-L-Leu⁷]didemnin B. In the following, we will demonstrate the potency of high-field NMR spectroscopy for the analysis of the extremely complicated mixture of four isomers (two rotamers each of two Lact epimers), *i.e.* [Me-L-Leu⁷]didemnin B (**A**/**B**) and [Me-L-Leu⁷, D-Lact⁹]didemnin B (**C**/**D**).

The synthesis of [Me-L-Leu⁷]didemnin B (**A**/**B**) and [Me-L-Leu⁷,D-Lact⁹]didemnin B (**C**/**D**) was carried out by the methods described [3] for the synthesis of didemnin B, which make possible the preparation of the didemnins and their analogs in decigram amounts. The synthesis of compounds analysed here and of other analogs as well as their cytostatic activity will be described in a subsequent report.

Assignment of the ^{1}H-NMR Resonances. – The proton resonances of [Me-L-Leu⁷]/[Me-L-Leu⁷,D-Lact⁹]didemnin B (**A**–**D**) could be assigned by using the following NMR experiments (500 MHz): DQF-COSY [8], TOCSY [9], NOESY [10], E.COSY [11], inverse H,C-COSY with TOCSY transfer [12] (the pulse sequence used in the latter experiment is shown in *Fig. 5b* (see below)), and 'inverse H,C-COLOC' with semisoft excitation by a *Gaussian*-shaped pulse [13]. The assignment procedure is very similar to the one recently described for didemnin A [5] and didemnin B [6], so we will concentrate on the special problems which arose from extreme complexity in the spectra of these epimers. *Fig. 2* shows the downfield NH part of the 500-MHz ^{1}H-NMR spectrum: the

NH resonances of the four different Leu^3 residues are nicely separated. Integration yields the relative ratio 57.0:24.4:15.1:3.5. Exact determination of these values is relevant for calibration and quantative analysis of the NOE signals as discussed later.

To proof the existence of four isomers, we have examined the NH *(Fig. 2)* and CH_3N part of the 500-MHz NOESY spectrum. The exchange cross-peaks Thr^{6}NH(**A**)/Thr^{6}NH(**B**), Thr^{6}NH(**C**)/Thr^{6}NH(**D**), Leu^{3}NH(**A**)/Leu^{3}NH(**B**), and Leu^{3}NH(**C**)/Leu^{3}NH(**D**) illustrated in *Fig. 2* give evidence for the existence of two pairs of conformers. In the CH_3N part of the NOESY spectrum, we again find exchange peaks only between **A** and **B** or **C** and **D**, but no exchange peaks between **A** and **C** or **D** (or **B** and **C** or **D**, resp.). We have checked the occurrence of the exchange peaks by a 500-MHz ROESY spectrum [14]. Positive cross-peak amplitudes exclude them to be NOE connectivities. Moreover, a 600-MHz ROESY spectrum of the independently synthesized [Me-L-Leu^7,D-Lact^9]-didemnin B (**C**/**D**) shows positive exchange peaks between the same pair of resonances for **C** and **D** as observed in the mixture **A**–**D** of the four isomers.

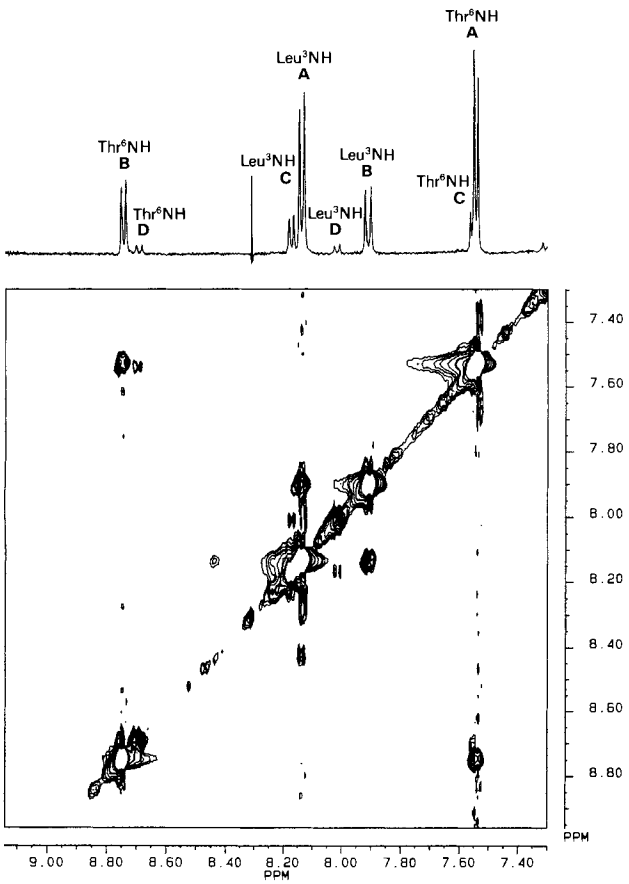

Fig. 2. *^{1}H-NMR spectra* (500 MHz) *of [Me-L-Leu^7]/[Me-L-Leu^7,D-Lact^9]didemnin B* (**A**–**D**) *in (D_6)DMSO: 1D-NMR and NOESY spectrum.* The NH part is shown without the Ist^1 NH resonances in the aromatic region.

Table 1. *^{1}H-NMR Chemical Shifts (δ) of [Me-L-Leu^7]Didemnin B (Conformation* **A***) in (D_6)DMSO Solution at 300 K*[a])

	Ist[1]	Hip[2]	Leu[3]	Pro[4]	Me_2Tyr[5]	Thr[6]	MeLeu[7]	Pro[8]	Lact[9]
NH	6.83 (7.18, 6.80, 7.30)	–	8.14 (7.91, 8.17, 8.01)	–	–	7.54 (8.75, 7.56, 8.69)	–	–	–
H–C(α)	3.35^S (3.33, 3.35)	3.90 (4.01)	4.48 (4.71, 4.46, 4.69)	4.54 (4.59)	4.07 (4.06)	4.51 (4.58, 4.69, 4.79)	5.04 (4.88, 5.13, 5.07)	4.77 (4.99)	4.31 (3.98, 4.35)
H′–C(α)	2.19^R (2.20, 2.19)	–	–	–	–	–	–	–	1.16 (1.17, 1.19)
CH_3–C(α)	–	1.11 (1.19)	–	–	–	–	–	–	–
H–C(β)[b])	3.78 (3.79, 3.78, 3.82)	–	1.38 (1.59^S, 1.38, 1.57)	2.08^S (2.17^S)	3.18^S	4.96 (4.98)	1.65^S (1.75, 1.60, 2.32)	2.20^S (2.13)	–
H′–C(β)[b])	–	–	1.38 (1.21^R, 1.38, 1.33)	1.53^R (1.53^R)	3.00^R	–	1.57^R (1.46, 1.60, 1.88)	1.72^R (1.70)	–
H–C(γ)[b])	3.83 (3.83, 3.78, 3.82)	4.94	1.51 (1.48, 1.51, 1.47)	1.95 (1.95)	–	1.08 (1.21)	1.53 (1.46, 1.48, 1.81)	2.03 (1.88)	–
H′–C(γ)	–	–	–	1.95 (1.95)	–	–	–	1.87 (1.88)	–
H–C(δ)	1.89	2.23	0.86 (0.89, 0.86, –[c]))	3.70 (3.65)	7.15	–	0.88 (0.89, 0.89, 0.88)	3.72 (3.83)	–
H′–C(δ)	–	–	0.83 (0.83, 0.83, –[c]))	3.49 (3.48)	–	–	0.78 (0.89, 0.80, 0.78)	3.48 (3.56)	–
CH_3–C(δ)	0.82	–	–	–	–	–	–	–	–
H–C(ε)	1.27	0.80	–	–	–	–	–	–	–
H′–C(ε)	1.11	0.74	–	–	6.86	–	–	–	–
CH_3(ξ)	0.84	–	–	–	–	–	–	–	–
CH_3N	–	–	–	–	2.53 (2.49)	–	2.98 (2.61, 2.90, 2.80)	–	–
CH_3O	–	–	–	–	3.73	–	–	–	–
OH	4.93 (4.88, 4.93)	–	–	–	–	–	–	–	4.76 (–[c]), 4.76)

[a]) The data of **B**–**D** are given in parentheses in the order of decreasing population: **B**, **C**, and **D**, resp. Superscripts *R* and *S* are used to indicate the diastereotopic assignment *(pro-R)* and *(pro-S)*.

[b]) For the isomers C and **D**, an arbitrary assignment is given for H–C(β), H′–C(β), and H–C(γ), of Leu^3 and MeLeu^7 because no distinction was possible for the two less populated isomers.

[c]) This value could not be obtained.

The ^{1}H-NMR chemical shifts of **A**–**D** are listed in *Table 1*. Not for all residues a set of four signals is observed. *E.g.*, the proton spin patterns of the two prolines (Pro) are only found twice, while the residues *N*,*O*-dimethyltyrosine (Me-Tyr(Me)[5]; short form,

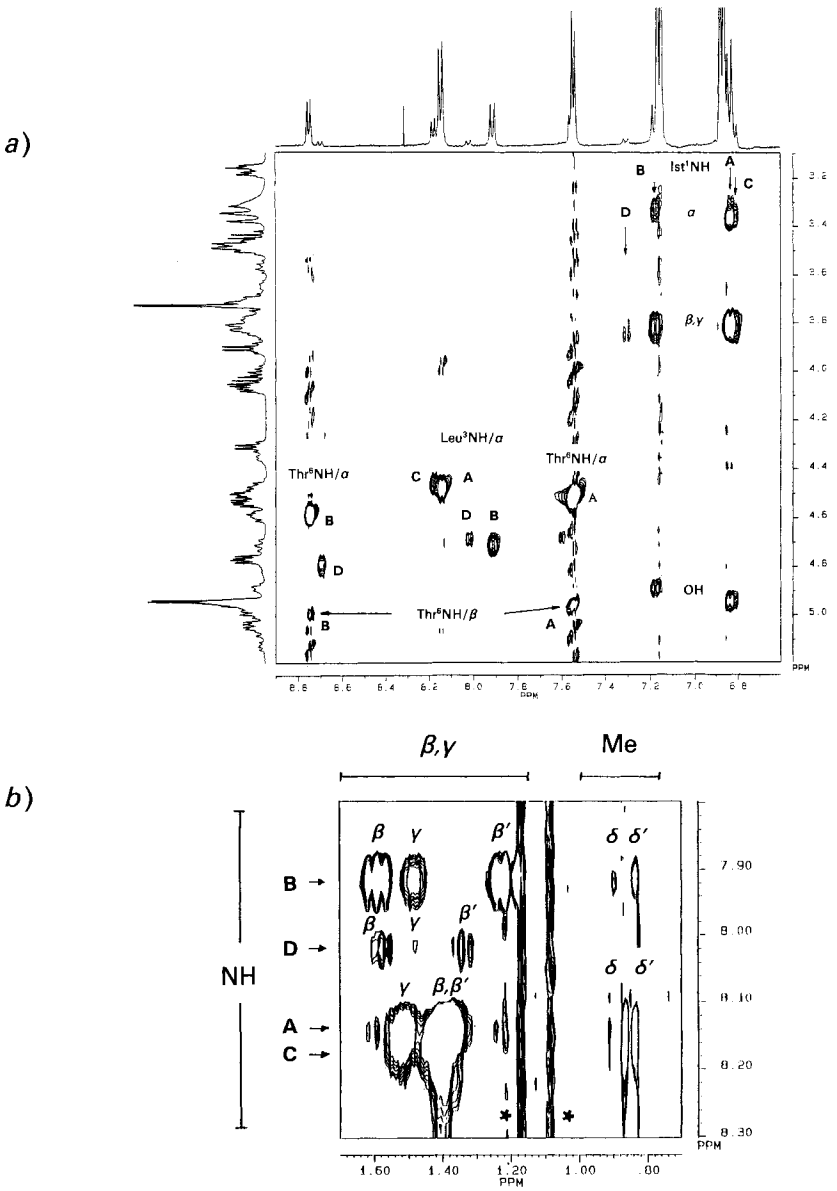

Fig. 3. a) *NH/H–C(α) part of the TOCSY spectrum* (500 MHz, mixing time 80 ms) *of [Me-*L*-Leu*^{7}*]/[Me-*L*-Leu*^{7}*,*D*-*Lact*^{9}*]didemnin B* (**A**–**D**) *in (D*$_6$*)DMSO.* α, β, and γ = α, β, and γ protons. Cross-peaks marked by arrows could be distinguished from t_1 ridges by comparison to the signals on the other side of the diagonal.

b) *High-field part of the Leu*^{3} *spin system in the same TOCSY spectrum as in* Fig. 3a. β,β′ = 2 H–C(β), γ = H–C(γ), δ,δ′ = 2 CH_3(δ). The two intensive lines marked by asterisks are artifacts.

Me_2Tyr^5) and hydroxyisovalerylpropionic acid (= (2*S*,4*S*)-4-hydroxy-2,5-dimethyl-3-oxohexanoic acid; Hip^2) are simply represented by one set of signals, with the exception of two signals for H–C(α) and the CH_3 group. The side chain of isostatin (= (3*S*,4*R*,5*S*)-4-amino-3-hydroxy-5-methylheptanoic acid; Ist^1) delivers the same resonances for all isomers, whereas the OH group exhibits three signals. Many other resonances exist as a set of four signals. In comparison to didemnin B [6], many more resonances of the less populated isomers can be assigned because of their higher populations. Examples will be given.

Fig. 3a shows the N*H*/*H*–C(α) part of the TOCSY spectrum. No difficulties arise to assign four distinct N*H* and *H*–C(α) resonances of the Ist^1, Leu^3, and Thr^6 residues. *Fig. 3b* shows the high-field part of the Leu^3 spin system in the same TOCSY spectrum. For the least populated conformer **D**, the assignment of the Leu^3 Me groups can not be achieved because of missing TOCSY peaks for the last transfer step.

The special difficulties in the differentiation between several Leu residues arising from the problem of detecting the connectivity between the β and γ protons was pointed out previously by us in the case of cyclosporin A [15]. There, heteronuclear long-range coupling was used to assign the Leu residues unambiguously. The limited amount of material prevented the application of COLOC to **A**–**D**, and the insufficient resolution in the C-dimension in a HMBC [16] experiment led us to apply another technique: we used the proton-detected H,C-COSY with TOCSY transfer [12] which in principle connects complete proton spin systems and represents them on C-atoms. This experiment allows the differentiation between the 2 *H*–C(β) and *H*–C(γ) resonances of Leu^3 and $MeLeu^7$ of **A** and **B**, respectively. This 'inverse' technique [12b] was employed without GARP decoupling [17] during detection thus exhibiting direct peaks as *doublets* in the proton dimension and relayed peaks as *singlets* which allows an easy distinction.

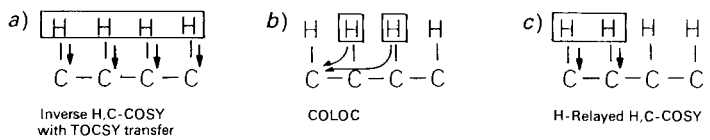

Fig. 4. *Connectivity patterns and the corresponding heteronuclear experiments used for their detection*

For comparison, *Fig. 4* shows the types of connectivity detected by different heteronuclear NMR techniques that do provide information about remote (*Fig. 4a* and *c*) or long-range (*Fig. 4b*) H,C connectivities. Method *a* joins the commonly used homonuclear TOCSY and the heteronuclear H,C-COSY into one experiment with additional improvement due to proton detection. We suppose this technique to be one of the most widely used methods for combined homo- and heteronuclear resonance assignments in the future. The way to evaluate such a spectrum will be described below in detail.

For the proton assignment of the CH_3N resonances, which represent separate spin systems, the 'inverse COLOC' experiment [13] was applied to detect long-range connectivities (see *Table 3* (below) for sequence assignments). The CH_3N proton assignment to the individual isomers was done by evaluation of the cross-peak intensities in the inverse H,C-COSY with TOCSY transfer. A proof of the assignment is given by the NOE data in *Table 6* (see below).

Assignment of the ^{13}C-NMR Resonances. – *Aliphatic C-Signals.* We used the following H-detected heteronuclear techniques which are more sensitive than conventional C-detected experiments: the inverse H,C-COSY (HMQC) [18] that delivers the direct connectivities and the inverse H,C-COSY with TOCSY transfer [12] whose advantages resulting from the additional remote connectivities were already mentioned (see *Fig. 4*).

Applying those two techniques, we assigned all C-resonances of the main conformer **A** and most of conformer **B**. With the exception of a few resonances, the sensitivity of the inverse experiments was not sufficient to determine the resonances of the two remaining isomers **C** and **D**.

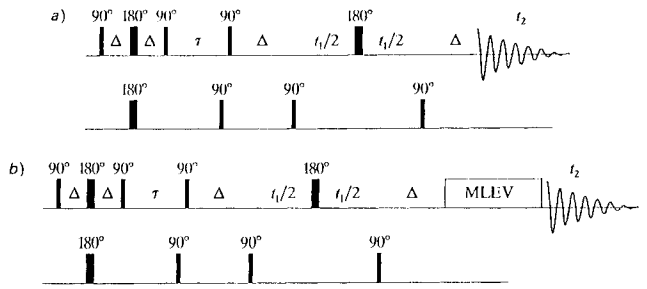

Fig. 5. a) *Pulse sequence of the proton-detected H,C-COSY.* b) *Sequence as in* a) *with additional TOCSY transfer step.*

The pulse sequence for the two experiments are shown in *Fig. 5*. In comparison to the 'classical' inverse H,C-COSY (HMQC) [19], three modifications in the applied sequence are used *(Fig. 5a): i)* the additional refocussing delay before aquisition, to achieve in-phase *doublets* in t_2 [12], *ii)* the sequence starts with a BIRD pulse which, after optimizing the delay τ, causes optimal suppression of proton signals from molecules without ^{13}C and enables rapid pulsing [12], and *iii)* the first $90°_{\zeta}$-^{13}C pulse ($\zeta = 0°, 180°$) eliminates longitudinal ^{13}C magnetization [12].

The ^{13}C-NMR chemical shifts of **A**–**D** are listed in *Table 2*, and the inverse H,C-COSY with TOCSY transfer spectrum is illustrated in *Fig. 6*. The additional remote connectivities lead to a large number of cross-peaks in the spectrum. The assignment procedure for the Thr^6 residue of conformers **A** and **B** is outlined in *Fig. 6*.

Starting with the chemical shift of the Thr^{6}N*H* resonance at 7.54 (**A**) and 8.75 (**B**) ppm, one follows horizontally at the chemical-shift line of Thr^6*C*(β) (68.9 and 69.6, resp.) until the direct Thr^6*H*–C(β) peak at 4.96 (**A**) and 4.98 (**B**) ppm is found. These peaks appear as *doublet*. Continuing at the Thr^6*C*(β) resonances, one gets the remote Thr^6*H*–C(α) peak at 4.51 (**A**) and 4.58 (**B**) ppm and at last the remote Thr^6*H*–C(γ) peak at 1.08 (**A**) and 1.21 (**B**) ppm, respectively. Drawing a line at the position of the center of the Thr^6*C*(β)/*H*–C(β) *doublet* perpendicular to the Thr^6*C*(β)-resonance line, one finds the remote Thr^6*C*(α)/*H*–C(β) peak at 54.9 (**A**) and 56.2 (**B**) ppm. Horizontally at the Thr^6*C*(α) resonance towards lower field, we find the Thr^{6}N*H* resonances again. Approaching the higher-field region horizontally at the Thr^6*C*(α) chemical shift, we first come to the direct Thr^6*H*–C(α) peak again which is represented as a *doublet* now and then to the remote signal of Thr^6*H*–C(γ). Following vertically at the Thr^6*H*–C(α) resonance brings us to the Thr^6*C*(γ) resonance at 14.5 (**A**) and 15.6 (**B**) ppm, respectively. The horizontal line at the Thr^6*C*(γ) chemical shift delivers again all proton resonances with the exception of the Thr^6*NH* peak. Summing up, one can say: at every C chemical shift, we find all H resonances on a horizontal line and at every H chemical shift, we find all the C resonances on a vertical line. A similar assignment procedure is done for the spin systems of the other amino acids, the starting points being outlined in *Fig. 6* for Leu^3 and Ist^1 of conformer **A** and **B**.

To find out if *cis*/*trans* proline isomerism of the peptide bond to Pro^4 or Pro^8 is responsible for the two conformers **A** and **B** of [Me-L-Leu^7]didemnin B, we checked the Pro*C*(β) Pro*C*(γ) resonances whose ^{13}C-NMR chemical shift give evidence for *cis* or *trans*

Table 2. *^{13}C-NMR Chemical Shifts (δ) of [Me-L-Leu^7]Didemnin B (Conformer A) in (D_6)DMSO Solution at 300 K*[a])

	Ist[1]	Hip[2]	Leu[3]	Pro[4]	Me_2Tyr^{5b})	Thr[6]	MeLeu[7]	Pro[8]	Lact[9]
C(α)	39.3 (38.8)	48.0 (47.6)	48.5 (48.5)	56.2 (55.5)	64.0	54.9 (56.2)	54.5 (57.4, 47.0, 53.8)	56.8 (56.2)	64.7 (65.0)
CH_3–C(α)	–	14.2 (15.0)	–	–	–	–	–	–	19.8 (19.3)
C(β)	66.2 (65.8)	205.1	39.3 (41.2)	27.8 (28.7)	33.3	68.9 (69.6)	36.3 (37.0, 36.3, 35.7)	27.2 (27.2)	–
C(γ)	55.4 (54.5)	79.8 (79.6)	23.7 (–[a]))	24.6 (25.0)	129.6	14.5 (15.6)	23.2	24.2 (24.4)	–
C(δ)	33.7	29.4 (29.4)	23.2 (23.2)	46.3 (46.7)	130.5	–	23.7	46.6 (46.8)	–
C′(δ)	–	–	20.6 (20.5)	–	–	–	21.4	–	–
CH_3–C(δ)	13.8	–	–		–	–	–	–	–
C(ε)	27.0	18.6	–	–	113.6	–	–	–	–
C′(ε)	–	16.3	–	–	–	–	–	–	–
C(ξ)	11.6	–	–	–	158.0	–	–	–	–
CH_3N	–	–	–	–	38.0 (39.7)	–	30.5 (27.8, 29.7, 28.1)	–	–
CH_3O	–	–	–	–	54.9	–	–	–	–
C=O	171.0	169.0 (168.5)	170.0	169.8 (169.5)	168.8 (168.6)	167.9 (168.4, 169.7)	170.1 (170.5)	172.4	171.9

[a]) Explanation of the data in parentheses, see *Table 1.*

[b]) The aromatic resonances were assigned in accordance to didemnin A [5].

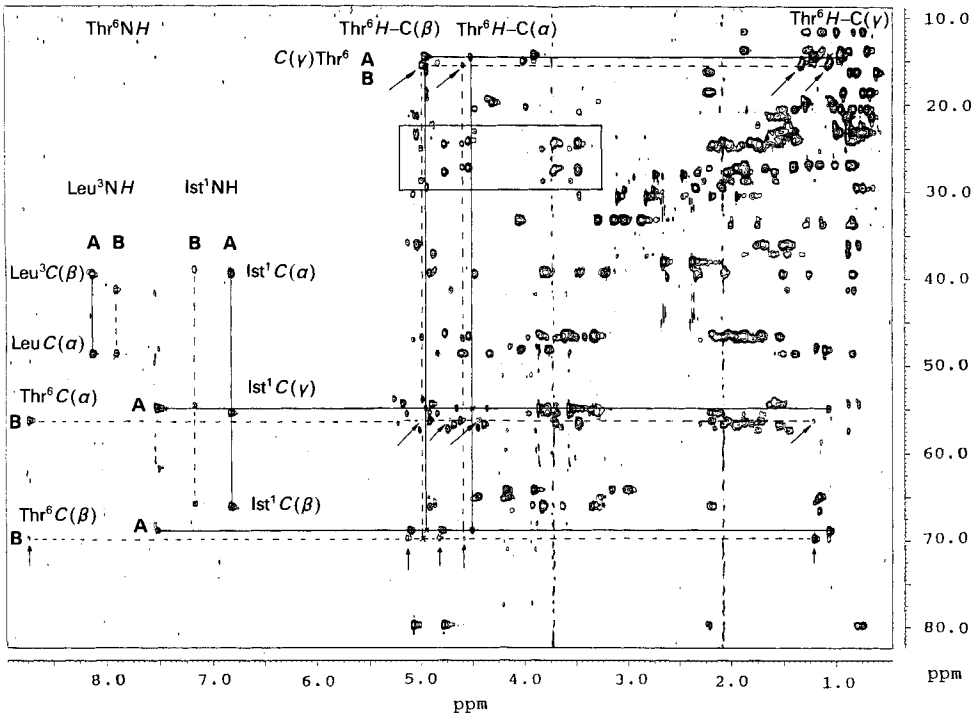

Fig. 6. *Inverse H,C-COSY with TOCSY transfer for [Me-L-Leu⁷]/[Me-L-Leu⁷,D-Lact⁹]didemnin B* (**A**–**D**) *in (D_6)DMSO recorded by the sequence of* Fig. 5b. The full assignment procedure for the Thr⁶ residues of **A** and **B** is given. Arrows indicate peaks from the second conformer. For the Ist¹ and Leu³ residues of **A** and **B**, the start of the assignment procedure is shown.

orientation about this bond [20] (typical values: *trans*-configurated prolines, 29.5 (C(β)) and 24.2 (C(γ)) ppm; *cis*-configurated prolines, 31.3 (C(β)) and 22.5 (C(γ)) ppm). The ^{13}C-NMR data of **A** and **B** *(Table 2)* prove *trans* peptide bonds for both Pro⁴ and Pro⁸. Thus, excluding this type of *cis/trans* isomerism, we assume, as already proven didemnin B [6], rotational isomerism about the secondary amid bond of *N*-methylated amino-acid residues giving rise to the existence of the different conformers. We will confirm this assumption below by discussing the results for the NOESY spectrum. A prerequisite of the conclusion concerning the *trans* peptide bonds to both Pro require an unambiguous assignment of the C(β) and C(γ) signals. Whereas this is not possible in the conventional C,H correlation (pulse sequence *Fig. 5a*), the additional TOCSY transfer, again, yields the desired information.

As it is obvious from *Fig. 6*, the spectral region between 24 and 29 ppm in F_1 and 1.50 and 2.05 ppm in F_2 showing direct $H-C(\beta)$ and $H-C(\gamma)$ connectivities of Pro⁴ and Pro⁸ is crowded preventing an unambiguous assignment of all $C(\beta)$ and $C(\gamma)$ signals to **A** and **B**. To gain the desired information, we analysed the expanded region of the spectrum marked in *Fig. 6* (see *Fig. 7*) which contains only remote connectivities (no splitting in the proton dimension) of the $C(\beta)$ and $C(\gamma)$ atoms. It is shown for the two Pro residues of **A** and **B**, how $H-C(\alpha)$, $H-C(\delta)$, and $H'-C(\delta)$ can be correlated to the $C(\gamma)$ and to the $C(\beta)$ resonances. This example clearly demonstrates, how the multistep H,H transfer facilitates the assignment procedure: The remote peaks are all *singlets* and most of them are nicely separated. In this part of the spectrum, a threefold check ($H-C(\alpha)$, $H-C(\delta)$, $H'-(\delta)$) of the C assignment is possible.

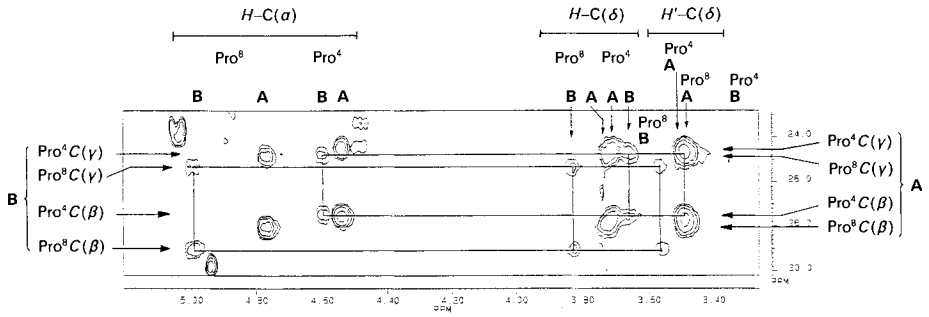

Fig. 7. *Part of the inverse H,C-COSY with TOCSY transfer spectrum of* **A**–**D** *in (D₆)DMSO (Fig. 6) showing only remote peaks of the Pro spin systems.* An unambiguous assignment of the $C(\beta)$ and $C(\gamma)$ resonances is possible excluding *cis/trans* Pro isomerism.

Carbonyl Resonances. To assign the CO resonances, we applied an 'inverse H,C-COLOC' spectrum with semisoft excitation of the CO resonances by a *Gaussian*-shaped pulse [13]. The cross-peak intensities of the main conformer **A** in this spectrum are strong enough to assign the CO resonances (see *Tables 2* and *3*) with the exception of Hip$^2C(\beta)$

Table 3. *Long-Range Correlations* (^2J (C,H) and ^3J (C,H)) *to the Carbonyl C-Atom for Sequence Assignments of the Amino-Acid Residues in the Isomers* **A**, **B**, *and* **C**

Isomer	Residue (CO)	COLOC correlations (H-atoms)			
A	Ist^1	Ist$^1H'$–C(α)	Ist^1H–C(α)	Hip^2H–C(γ)	
	Hip^2	Hip^2H–C(α)	Hip$^2CH_3$–C(α)	Leu^3H–C(α)	Leu^{3}NH
	Leu^3	Leu^3H–C(α)			
	Pro^4	Pro^4H–C(β)	Pro$^4H'$–C(β)	Me$_2$Tyr^{5}CH_3N	Me$_2$Tyr^5H–C(α)
	Me$_2$Tyr^5	Me$_2$Tyr^5H–C(α)	Me$_2$Tyr$^5H'$–C(β)	Thr^6H–C(β)	
	Thr^6	Thr^6H–C(α)	Thr^6H–C(β)	Ist^1H–C(γ)	Ist^{1}NH
	MeLeu^7	MeLeu^7H–C(α)	MeLeu^7H–C(β)	Thr^{6}H–C(α)	Thr^{6}NH
	Pro^8	Pro^8H–C(α)	Pro^8H–C(β)	Pro$^8H'$–C(β)	MeLeu$^7CH_3$N
	Lact^9	Lact^9H–C(α)	Lact^9–CH_3(β)		
B	Hip^2	Hip^2H–C(α)	Hip^2–CH_3–C(α)	Leu^{3}NH	
	Pro^4	Pro^4H–C(α)	Pro$^4H'$–C(β)	Me$_2$Tyr^5H–C(α)	Me$_2$Tyr$^5CH_3$N
	Me$_2$Tyr^5	Me$_2$Tyr^5H–C(α)	Thr^6H–C(β)		
	Thr^6	Thr^6H–C(α)	Thr^6H–C(β)		
	MeLeu^7	MeLeu^7H–C(α)	Thr^{6}NH		
C	Thr^6	Thr^{6}NH	MeLeu^7H–C(α)		

because this CO resonance at 205.1 ppm was not included in the excitation range of the *Gaussian* pulse to increase the resolution in F_1. For the second conformer **B**, the assignment of five CO resonances is possible, and even for the third isomer **C**, a correlation from Thr^6CO to MeLeu^7H–C(α) and to Thr^{6}NH appears in the spectrum. Using the long-range correlations listed in *Table 3*, sequence assignments of the different Pro in **A** and **B** can be done.

Sequence Analysis. – Having a mixture of the four isomers **A**–**D**, a special question arises: which set of resonances belongs to which isomer? Usually, resonance assignments are made with the reasonable assumption, that the cross-peak intensities are proportional

to the amount of the different isomers. However, because these intensities also depend on the transfer functions [21], a careful check of the so obtained preliminary assignment by sequence analysis for isomers **A** and **B** was done. Starting with the Leu[3] residue for sequence determination (from the 1D ^{1}H-NMR spectrum (see *Fig. 2*), it is known which Leu[3] spin pattern belongs to which isomer), we can walk around the whole ring using the COLOC correlations of the main conformer **A** (see *Table 3*). For conformer **B**, correlations are missing between the residues Ist[1] and Thr[6], Leu[3] and Pro[4], and Ist[1] and Hip[2] (*Table 3*). However, the first two sequency pairs can be identified by NOE connectivities. NOESY cross-peaks are found between Ist[1]N*H* and Thr[6]*H*–C(α) as well as between Pro[4]*H*–C(γ) and Leu[3]$H_{(pro\text{-}S)}$–C(β) and Pro[4]*H*–C(α) and Leu[3]*H*–C(δ).

Extraction of Conformationally Relevant NMR Parameters for Conformers A and B. – Conformational analysis was performed by the determination of chemical-shift values, the temperature dependence of N*H* chemical-shift values (*Table 4*), and by determination of vicinal H,H-coupling constants from the 1D ^{1}H-NMR spectrum and the E.COSY [11] spectrum. The coupling constants are listed in *Table 5*. *Fig. 8* shows the part of the E.COSY spectrum that was used to extract the $J(H\text{–}C(\alpha), H\text{–}C(\beta))$ of the Pro residues of the two conformers **A** and **B**.

In addition, a quantitative evaluation of NOE cross-peak intensities was done in a 500-MHz NOESY spectrum with a mixing time of 120 ms. Exact evaluation of the NOE

Table 4. *Temperature Dependence of the NH Chemical Shifts, Given as* $-\Delta\delta/\Delta T$ [ppb/K]

Isomer	$-\Delta\delta/\Delta T$		
	Ist[1]	Leu[3]	Thr[6]
A	0.3	3.8	4.9
B	1.0	1.8	4.5
C	1.0	5.0	5.5
D	2.3	3.5	6.4

Table 5. ^3J(H,H) *Coupling Constants of Isomer* **A**[a])

Residue	^3J(N*H*, *H*–C(α))[b])	$^3J(H\text{–}C(\alpha), H\text{–}C(\beta))$[c])	$^3J(H\text{–}C(\alpha), H\text{–}C(\beta))$[c])
Ist[1]	[d])	[e])	–
Hip[2]	–	4.01[f])	–
Leu[3]	8.1 (9.4, 8.1, 9.1)	[e]) (2.2)	[e]) (11.1)
Pro[4]	–	4.5 (5.8)	8.9 (8.9)
Me_2Tyr[5]	–	11.1 (11.1)	4.9 (4.9)
Thr[6]	[e]) (7.47, [e]), 9.4)	< 5	–
MeLeu[7]	–	4.9 (8.0, 8.9)	10.3 (6.2)
Pro[8]	–	4.9 (5.8)	8.5 (7.6)
Lact[9]	–	[e])	–

[a]) In parentheses, the data of isomers **B**–**D** are given in the order of decreasing population: **B**, **C**, and **D**, respectively.

[b]) Determined from the 1D spectrum after *Lorentz* to *Gauss* transformation.

[c]) Determined from the E.COSY spectrum.

[d]) ^3J(N*H*, *H*–C(γ)) not determined.

[e]) Not determined.

[f]) Here: $^3J(H\text{–}C(\gamma), H\text{–}C(\delta))$.

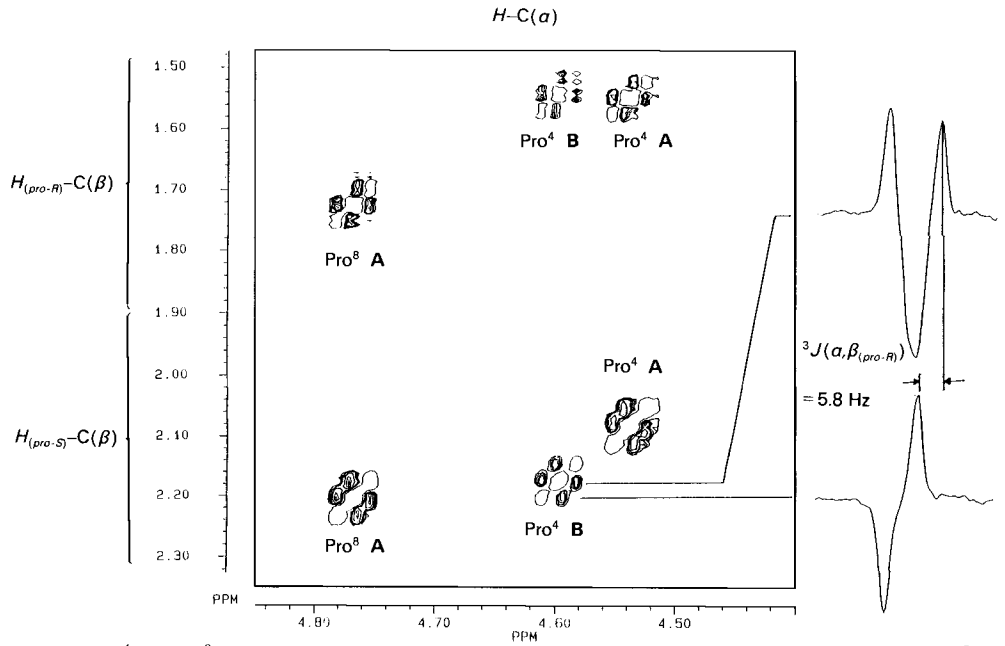

Fig. 8. *Pro⁴ and Pro⁸* H–*C*(α)/H–*C*(β) *cross-peak region of the 500-MHz E.COSY spectrum of [Me-*L*-Leu⁷]-didemnin B* (**A**/**B**) *in* (D_6)*DMSO*. Negative levels are indicated by only one contour line. Extraction of the $^3J(\alpha,\beta)$ values followed the usual way and is demonstrated for one coupling constant of the second conformer **B**.

cross-peak intensities was not so easy as expected due to overlapping cross-peaks for the different isomers. First of all, we had to find a suitable NOE cross-peak as reference for H,H-distance (r(H,H)) calibration. For conformer **A**, we took the Thr⁶*H*–C(β)/*H*–C(γ) correlation whose integral had to be diminished by the contribution of the overlapping cross-peak of isomer **C**.

At the first glance, the H,H-distance calibration seems to be very important for the total result of the corresponding molecular dynamics (MD) refinement. However, if the calibration is incorrect, one observes a systematic deviation of all calculated distances in the MD refinement. Hence, the results of the calculation are also useful if the calibration is incorrect. In our case, the values obtained in this process (see *Table 6*) show good agreement for the calculated and observed distances ($r(H,H)^{MD}$ and $r(H,H)^{NOE}$, resp.). Thus, a correction of the calibration as it was done in other cases where no suitable cross-peak for calibration was available [22] is not necessary. As a first approximation, we made the assumption that the contributions to the NOE cross-peak intensity of **A** and **B** are related in the same proportion as their populations are. Expanding this assumption to all overlapping NOE correlations of the different isomers, we had to correct the experimental integration values of overlapping signals in this sense by subtraction of the signals of the not relevant isomers. The NOE connectivity Leu³N*H*/Leu³*H*–C(α) which represents only conformer **B** served as reference for this conformer. The NOE connectivities of the two remaining isomers **C** and **D** were not evaluated quantitatively. All experimental and MD calculated distance values are listed in *Table 6*.

Table 6. *Comparison of Experimental* (NOESY) *and Calculated* (Molecular Dynamics) *H,H Distances for the Two Conformers* **A** *and* **B** *of [Me-L-Leu^7]Didemnin B*

Involved protons		Conformer **A**		Conformer **B**	
		r (H,H)^{NOE}	r (H,H)^{MD}	r (H,H)^{NOE}	r (H,H)^{MD}
Ist^{1}N*H*	Ist$^1H_{(pro\text{-}S)}$–C(α)	256	305	–	–
Ist^{1}N*H*	Ist^1H–C(β)	–	–	233	247
Ist^{1}N*H*	Thr^6H–C(α)	211	208	219	212
Ist^{1}N*H*	Hip$^2CH_3$(ε)	–	–	463	553
Ist$^1H_{(pro\text{-}S)}$–C(α)	Hip^2H–C(δ)	295[a])	407	–	–
Ist^1H–C(β)	Ist$^1H_{(pro\text{-}S)}$–C(α)	260	293	–	–
Ist^1H–C(γ)	Ist$^1H_{(pro\text{-}R)}$–C(α)	278	375	287	274
Ist^1H–C(γ)	Ist^1H–C(δ)	254	251	249	244
Ist^{1}O*H*	Ist^1H–C(δ)	336	364	–	–
Hip^2H–C(α)	MeLeu$^7H_{(pro\text{-}R)}$–C(β)	287	316	–	–
Hip^2H–C(γ)	Hip^2H–C(δ)	275	241	284	296
Leu^{3}N*H*	Leu^3H–C(α)	300[c])	294	300[d])	289
Leu^{3}N*H*	Leu^3H–C(β)	259	263	254[R]	362
Leu^{3}N*H*	Hip^2H–C(α)	218	212	224	220
Leu^{3}N*H*	Pro^4H–C(δ)	338[b])	458	–	–
Leu^{3}N*H*	Ist$^1H_{(pro\text{-}S)}$–C(α)	277	315	325	406
Leu^{3}N*H*	Hip$^2CH_3$–C(α)	302[a])	398	–	–
Leu^3H–C(α)	Pro^4H–C(δ)	218	209	–	–
Leu^3H–C(β)	Leu$^3CH_3$(δ)	255[a])[b])	314	–	–
Leu^3H–C(γ)	Leu$^3CH_3$(δ)	240[a])[b])	245	–	–
Pro^4H–C(α)	Pro$^4H_{(pro\text{-}S)}$–C(β)	241	234	268	245
Pro^4H–C(α)	Me$_2$Tyr$^5CH_3$N	215	229	246	236
Pro^4H–C(α)	Leu^3H–C(δ)	–	–	233[a])	432
Pro^4H–C(γ)	Leu$^3H_{(pro\text{-}S)}$–C(β)	–	–	236[b])	360
Pro$^4H'$–C(δ)	Leu^3H–C(β)	242[b])	449	–	–
Me$_2$Tyr^5H–C(α)	Me$_2$Tyr$^5H_{(pro\text{-}S)}$–C(β)	250	247	258	257
Me$_2$Tyr^5H–C(α)	Me$_2$Tyr$^5CH_3$N	227	236	234	232
Me$_2$Tyr$^5CH_3$N	Leu$^3H'$–C(δ)	237[a])	463	242[a])[a])	438
Me$_2$Tyr$^5CH_3$N	Pro$^4H_{(pro\text{-}R)}$–C(β)	267[a])	411	–	–
Thr^{6}N*H*	Thr^6H–C(α)	267	280	313	277
Thr^{6}N*H*	Thr^6H–C(β)	264	263	238	238
Thr^{6}N*H*	Thr^6H–C(γ)	266	296	269	312
Thr^{6}N*H*	Leu^3H–C(β)	421	486	–	–
Thr^{6}N*H*	MeLeu^7H–C(α)	239	264	254	231
Thr^{6}N*H*	MeLeu$^7CH_3$N	322[a])	324	–	–
Thr^6H–C(α)	Leu^3H–C(β)	258[b])	366	–	–
Thr^6H–C(β)	Thr^6H–C(α)	233	245	–	–
Thr^6H–C(β)	Thr^6H–C(γ)	240[d])	241	–	–
Thr^6H–C(β)	Lact^9H–C(α)	–	–	228	233
MeLeu$^7CH_3$N	MeLeu^7H–C(γ)	286[a])	320	–	–
Pro^8H–C(α)	MeLeu^7H–C(α)	–	–	200	163
Pro^8H–C(α)	MeLeu$^7CH_3$N	231	238	–	–

[a]) Increased by 100 pm for MD run (CH_3 group [26]).

[b]) Increased by 90 pm for MD run, because of the lack of diastereotopic assignment [26].

[c]) Was corrected up to 300 pm considering the ^3J(N*H*,*H*–C(α)).

[d]) Calibration distance.

For conformer **B**, one observes a distinct NOE cross-peak between MeLeu^7*H*–C(α) and Pro^8*H*–C(α) (see *Fig. 9*) indicating a *cis* peptide bond between these residues. Note that the numbering of the three amino acids in the side chain of [Me-L-Leu^7]didemnin B (see *Fig. 1*) is reversed as compared to the normal numbering of peptide sequences (from N-terminal to the C-terminal end). Hence, the *cis* peptide bond Pro^8-MeLeu^7 does not cause the C(β) and C(γ) shifts in the ^{13}C-NMR typical for *cis* proline [20] as mentioned above! Because of overlap (see exchange peak 1 in *Fig. 9*), no attempt was made to get the volume integral of this *H*–C(α)/*H*–C(α) NOE signal (peak 2). In accordance with [23] [24], a H,H distance of 200 pm served as the input value of this distance for structure refinements by MD calculation.

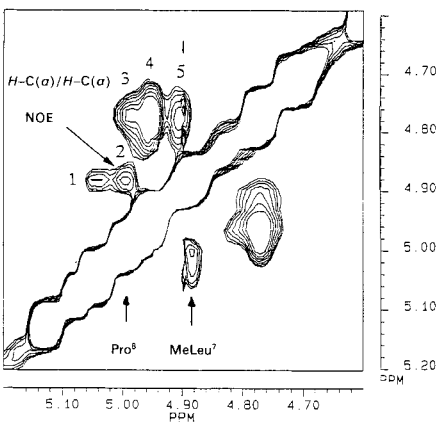

Fig. 9. *Part of the 500-MHz NOESY spectrum of [Me-L-Leu^7]/[Me-L-Leu^7,D-Lact^9]didemnin B* (**A**–**D**) *in (D$_6$)DMSO.* The MeLeu^7 *H*–C(α)/Pro^8 *H*–C(α) NOE cross-peak of conformer **B** (peak 2), verifying the *cis* peptid bond in **B**, is indicated by an arrow. The residual peaks 1,3 and 4,5 are exchange peaks (*H*–C(α) of **A**/*H*–C(α) of **B** and O*H*/O*H*, resp.) which could be confirmed by positive cross-peak amplitudes in a 500-MHz ROESY spectrum.

Determination of the Solution Structure of Conformers A and B by MD Calculation. – The MD calculations were performed using the GROMOS [25–27] program system. The force field is specially parameterized for peptides and nucleic acids. The starting coordinates were taken from the recently solved X-ray structure of didemnin B [7] with additional conversion of the C(α) configuration of MeLeu^7. After energy minimization, we performed a 50 ps restrained MD run. The temperature gradients of the N*H* chemical shifts were implemented as factors reducing the charges of the solvent-exposed N*H* [28]: full charge was left at the temperature gradient of 0.3 ppb/K for Ist^{1}N*H* of **A**, whereas for Thr^{6}N*H* of **A** ($\Delta\delta/\Delta t = 4.9$ ppb/K), a reduction to 25% was used. Intermediate values were linearily interpolated. The MD run consisted of two different steps: 5 ps at 300 K with a strong coupling to the temperature bath [29], followed by 45 ps at 300 K with a weak coupling to the bath. The applied force constant for the restraint was 2000 KJ mol^{-1} nm^{-2}. Besides this, the MD calculation was performed as described before [6] [28]. The same procedure was applied to the second conformer **B** by using its individual set of constraints, though in one point the procedure differentiated. We turned the Pro^8-MeLeu^7 peptid bond from *trans* to *cis* in the starting structure because of the

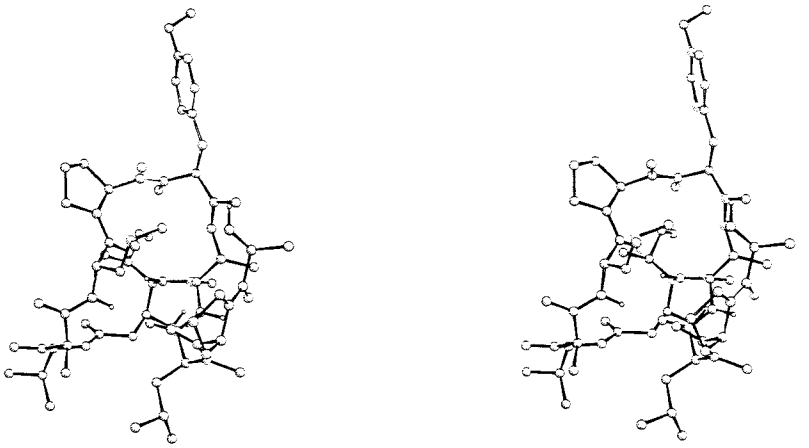

Fig. 10. *Stereoview of the mean trajectory of [Me-L-Leu⁷]didemnin B* (conformer **A**) *obtained by 50 ps restrained MD calculation (in vacuo)*

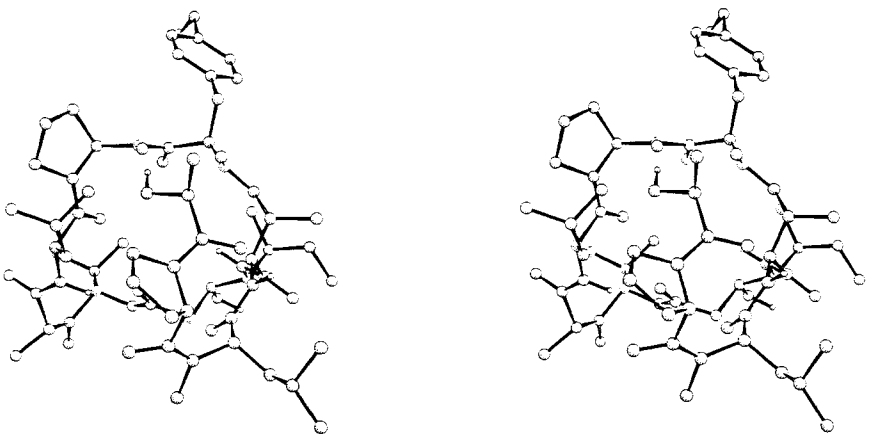

Fig. 11. *Stereoview of the mean trajectory of [Me-L-Leu⁷]didemnin B* (conformer **B**) *obtained by 50 ps restrained MD calculation (in vacuo)*

Pro⁸*H*–C(α)/MeLeu⁷*H*–C(α) NOE. The trajectory from 5 to 50 ps was used to derive a 'mean' conformation for **A** *(Fig. 10)* and for **B** *(Fig. 11)* as usual [6] [27].

Comparison of the Solution Structure of Conformer A of [Me-L-Leu⁷]Didemnin B with the Solution and Crystal Structure of Didemnin B. – Similarly to didemnin B, its epimer [Me-L-Leu⁷]didemnin B is not homogeneous on the time scale of the NMR experiment, but in contrast to didemnin B where three conformations in a ratio of 8:1:1 were observed, [Me-L-Leu⁷]didemnin B exhibits only two conformations, allowing to obtain sufficient NMR parameters to perform a conformational analysis for both, **A** and **B**.

First, we will concentrate on the most populated conformer **A** of [Me-L-Leu⁷]-didemnin B. The 23-membered ring is folded like a bend 'figure-of-eight' as in the case of didemnin B. The ring structure is stabilized by a transannular H-bridge that links Ist¹N*H* and Leu³C*O*, though the population during the MD run of this H-bond is a bit lower

Table 7. *Comparison of the MD-Calculated H-Bonds of [Me-L-Leu⁷]Didemnin B* (Conformer **A** and **B**) *and of Didemnin B, Including the Values of the X-Ray Structure of Didemnin B*

Hydrogen bridge[a])			[Me-L-Leu⁷]Didemnin B		Didemnin B	
Donor	Acceptor		Conformer **A** (MD)	Conformer **B** (MD)	MD	X-ray
Ist¹N*H*	Leu³CO	r[pm]	293	284[b])	280	302
		θ[deg]	143	144[b])	158	142
		P[%]	85	94[b])	99	–
Leu³N*H*	MeLeu⁷C*O*[c])	*r*[pm]	289	–[d])	290	291
		θ[deg]	153	–	162	169
		P[%]	99	–	100	–
Thr⁶N*H*	Lact⁹C*O*	*r*[pm]	329	297	289	309
		θ[deg]	136	135	152	156
		P[%]	63	42	96	–
Lact⁹O*H*	Me_2Tyr⁵C*O*	*r*[pm]	317	315	296	433[d])
		θ[deg]	146	133	159	–
		P[%]	71	38	90	–
Ist¹O*H*	Thr⁶C*O*	*r*[pm]	311	–[d])	–[d])	–[d])
		θ[deg]	144	–	–	–
		P[%]	51	–	–	–

[a]) Definition of H-bonds: distance *r*, angle θ and population *P* as described before [6].
[b]) Donor Leu³N*H* and acceptor Ist¹C*O*.
[c]) Me-D-Leu⁷C*O* in the case of didemnin **B**.
[d]) H-Bridge not apparent here.

(85%) than the same bond in didemnin B (99%, *Table 7*). The temperature dependence of the Ist¹N*H* chemical shift is very similar to the one of didemnin B: a small value (0.3 ppb/K for **A** and 0.5 ppb/K for didemnin B, see *Table 4*) clearly indicates the intramolecular H-bridge. The second H-bond involving Leu³N*H* and MeLeu⁷C*O* (**A**) or Me-D-Leu⁷C*O* (didemnin B) is responsible for the back folding of the linear moiety towards the ring system. The population of this H-bond during the MD calculation is the same for **A** and didemnin B (99 and 100%, resp.), though the temperature gradient of the Leu³N*H* (3.8 ppb/K) is not as small as the one for didemnin B (1.8 ppb/K). The third H-bond observed in didemnin B between Thr⁶N*H* and Lact⁹C*O* is involved in the βII turn with Pro⁸ in the $i + 1$ and Me-D-Leu⁷ in the $i + 2$ position. This H-bond is only populated by 63% during the MD run of **A** (see *Table 7*).

It is obvious from the calculated dihedrals (see *Table 8*) and the *Ramachandran* diagrams in *Fig. 12* that the conformational requirements for the βII-turn structure are fulfilled for **A** as good as for didemnin B, though the chirality at C(α) of MeLeu⁷ is reversed. Normally, one expects a conformational change when an L-amino acid is substituted by a D-configurated residue. On the other hand, often the overall conformation is retained and only a small region such as a βII′ turn changes to a βII turn. *E.g.*, cyclo(-Xaa-Phe_2-D-Pro-Phe_2-) where Xaa is L-Pro or D-Pro adopts conformations with a βII′ about D-Pro-Phe, but a βII about L-Pro-Phe [30]. Similar results are obtained in cyclo (-D-Pro-Phe-Thr-Lys-Xaa-Phe-) with Xaa = L-Trp or D-Trp [30]. In conformer **A**, the described βII-turn structure could be confirmed by two NOE effects: one between Pro⁸*H*–C(α) and MeLeu⁷CH_3N which was stronger (distance 231 pm) than in didemnin B (distance 286 pm), and one between MeLeu⁷CH_3N and Thr⁶N*H* (distance 322 pm for **A** and 260 pm for didemnin B). The third weak NOE connectivity Thr⁶N*H*/Pro⁸*H*–C(α)

Table 8. *Comparison of the MD-Calculated Backbone Dihedrals in the Macrocyclic Ring and in the Linear Peptide Side-chain of [Me-L-Leu7]Didemnin B* (Conformer **A** and **B**) *and of Didemnin B, Including the Dihedrals of the X-Ray Structure of Didemnin B*

Residue	Dihedral angle	[Me-L-Leu^7]Didemnin B		Didemnin B	
		Conformer **A** (MD)	Conformer **B** (MD)	MD	X-ray
Ist^1	CO–N–C(γ)–C(β)(ϕ)	98	137	122	113
	N–C(γ)–C(β)–C(α)(ψ)	44	–53	–60	–58
	C(γ)–C(β)–C(α)–CO	90	134	168	164
	C(β)–C(α)–CO–O	–152	79	–151	166
Hip^2	C(α)–CO–O–C(γ)	–175	–175	179	177
	CO–O–C(γ)–C(β)	–154	–102	–123	–142
	O–C(γ)–C(β)–C(α)	–18	94	–26	39
	C(γ)–C(β)–C(α)–CO	117	41	112	60
	C(β)–C(α)–CO–N(ψ)	–117	–98	–130	–134
	C(α)–CO–N–C(α)(ω)	–175	180	–173	–167
Leu^3	CO–N–C(α)–CO(ϕ)	–123	–101	–110	–124
	N–C(α)–CO–N(ψ)	136	176	148	158
	C(α)–CO–N–C(α)(ω)	172	168	164	174
Pro^4	CO–N–C(α)–CO(ϕ)	–76	–75	–68	–75
	N–C(α)–CO–N(ψ)	118	116	149	163
	C(α)–CO–N–C(α)(ω)	–175	173	–176	178
Me_2Tyr^5	CO–N–C(α)–CO(ϕ)	92	54	52	51
	N–C(α)–CO–O(ψ)	60	111	56	84
	C(α)–CO–O–C(α)	–163	–177	–170	–121
Thr^6	CO–O–C(β)–C(α)	124	108	129	152
	O–C(β)–C(α)–CO	–165	–155	–153	–155
	C(β)–C(α)–CO–N(ψ)	79	140	121	156
	C(α)–CO–N–C(γ)(ω)	–172	–179	–176	–178
	C(β)–C(α)–N–CO(ϕ)	–74	–63	–48	–68
MeLeu^{7a})	C(α)–CO–N–C(γ)(ω)	178	–178	179	–170
	N–C(α)–CO–N(ψ)	47	138	–18	–29
	CO–N–C(α)–CO(ϕ)	58	–108	112	103
Pro^8	C(α)–CO–N–C(α)(ω)	–178	–7	–164	180
	N–C(α)–CO–N(ψ)	118	99	120	124
	CO–N–C(α)–CO(ϕ)	–61	–107	–53	–63
Lact^9	C(α)–CO–N–C(α)(ω)	179	177	–177	–169
	C(β)–C(α)–CO–N(ψ)	–46	–36	121	158

[a]) Me-D-Leu in the case of didemnin B.

that is indicative for the βII turn in didemnin B (distance 353 pm), and should account for an even shorter distance in its Me-L-Leu^7 derivative **A** could not be observed in the latter case, probably because of the smaller signal/noise level in our measurement. We observed two additional H-bonds for **A**: the side chain stabilizing H-bond between Lact^{9}O*H* and Me_2Tyr^{5}C*O* that was already observed for didemnin B in solution but not in the crystalline state, and a H-bridge between Ist^{1}O*H* and Thr^{6}C*O* which was not found for didemnin B before and might be an artifact caused by vacuum effects in the calculation.

The same two unconventional βII turns described for didemnin B were found also for **A**. The first βII turn involves Thr^6 in the $i+1$ and Ist^1 in the $i+2$ position. Although H-bond formation is not possible, the turn type in **A** can be described even better by a βII-turn type than in didemnin B itself because the deviation ($\Delta\psi = 44°$) of the calculated

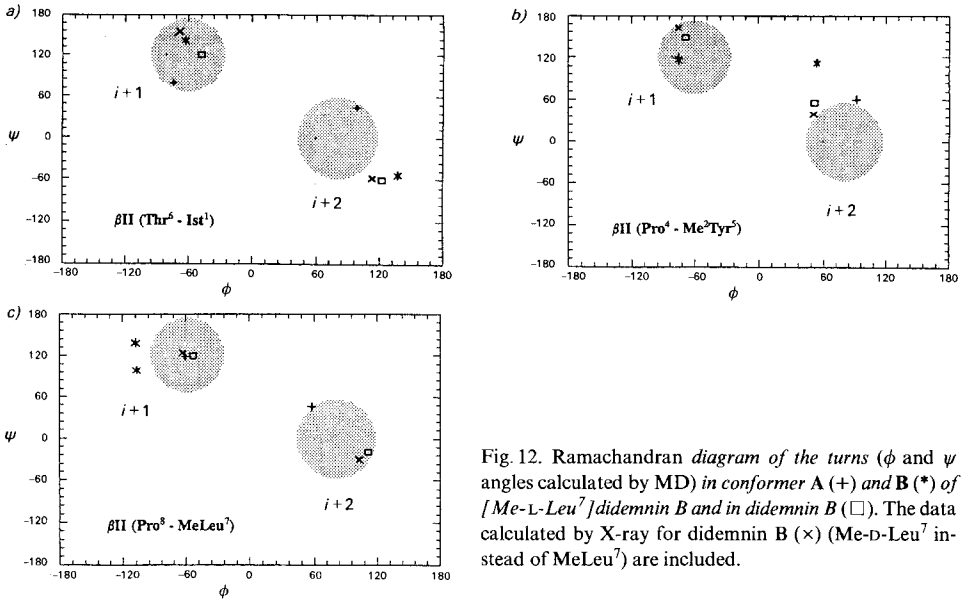

Fig. 12. Ramachandran *diagram of the turns* (ϕ and ψ angles calculated by MD) *in conformer* **A** (+) *and* **B** (*) *of [Me-L-Leu⁷]didemnin B and in didemnin B* (□). The data calculated by X-ray for didemnin B (×) (Me-D-Leu⁷ instead of MeLeu⁷) are included.

ψ dihedral angle for Ist¹ from its ideal value ($\psi = 0$) is smaller in **A** than in didemnin B ($\Delta\psi = 60°$). This can be visualized in the *Ramachandran* diagram in *Fig. 12a*. The following NMR data will confirm our assumption of the turn structure: *i*) The Leu³N*H*/Ist¹ $H_{(pro\text{-}S)}$–C(α) NOE is observed in **A** as well as in didemnin B (277 and 264 pm, resp.). *ii*) The Ist¹N*H*/Thr⁶*H*–C(α) NOE with 211 and 210 pm in **A** and didemnin B, respectively, accounts for a very similar structure in both molecules and confirms Thr⁶ being involved in the $i + 1$ position of the βII turn type. *iii*) A small $J(H\text{–C}(\alpha), H\text{–C}(\beta))$ value for Thr⁶ was already expected from the X-ray structure of didemnin B, and we find it again in **A** (see *Table 5*). As shown in *Fig. 12a*, the requirements for the torsion angles of Thr⁶ for the assumed turn type are fulfilled satisfactorily.

The second nonclassical βII turn involves Pro⁴ ($i + 1$ position) and Me_2Tyr⁵ ($i + 2$ position). The bond from Me_2Tyr⁵ to Thr⁶ is a lacton instead of an amide bond. The following NOE pattern *(cf. Table 6)* strengthen the assumption of the turn type (for comparison, data of didemnin B are given in parentheses). Me_2Tyr⁵CH_3N/Me_2Tyr⁵*H*–C(α) NOE with 227 (204) pm, Me_2Tyr⁵CH_3N/Pro⁴*H*–C(α) NOE with 215 (192) pm; and Leu³N*H*/Ist¹$H_{(pro\text{-}S)}$–C(α) NOE with 277 (264) pm. A view onto the *Ramachandran* plots in *Fig. 12b* indicates again that the deviations of the MD-calculated values from the ideal values for the torsion angles (Pro⁴: $\phi = -60°$ and $\psi = 120°$; Me_2Tyr⁵: $\phi = 80°$ and $\psi = 0°$) are similar for **A** and didemnin B (solution structure by MD and crystal structure).

Summing up, one can say that there exists a near equivalence of the solution structure of conformer **A** and didemnin B. The r.m.s. deviations for positional fluctuations of selected backbone atoms during the MD calculations confirm the prediction of a fairly rigid ring system in [Me-L-Leu⁷]didemnin B (conformer **A**), as in the case of didemnin B (see *Fig. 13*). Distinct higher fluctuations for Hip²C(γ), as shown for didemnin B, could

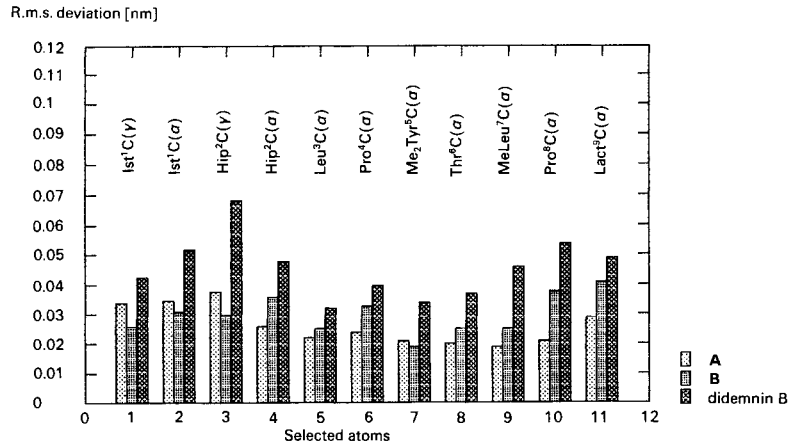

Fig. 13. *R.m.s. deviations* [nm] *from the mean atomic positions of selected atoms of conformer* **A** *and* **B** *of [Me-L-Leu⁷]didemnin B and of didemnin B* (Me-D-Leu⁷ instead of MeLeu⁷)

not be observed for [Me-L-Leu⁷]didemnin B which might be a consequence of the 'pushed away' Ist¹-Hip² part of the molecule by the Me-L-Leu⁷ residue (see below) resulting in a better definition of this region. As *Fig. 13* shows, the MeLeu⁷-Pro⁸-Lac⁹ side chain is quite well defined as well.

Despite the close analogy of the structures of **A** and didemin B, there exists a distinct difference in the orientation of the Ist¹-Hip² region which points more towards the outer side of the ring in **A**, thus giving rise to a more expanded ring system in this amino-acid region (see *Fig. 14*). This may be caused by the influence of the linear side-chain moiety:

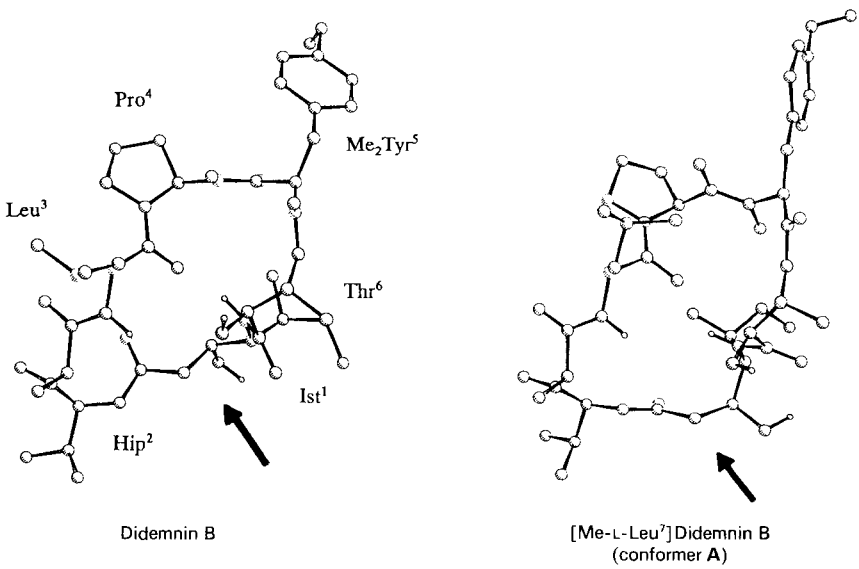

Fig. 14. *Comparison of the 'mean' conformations of didemnin B and conformer* **A**. The arrows indicate the region where the change in the ring structure occurs. For the sake of clarity, the linear side chain consisting of MeLeu⁷-Pro⁸-Lac⁹ is omitted.

Assuming (see below) a χ_1 dihedral angle of $-60°$ for Me-L-Leu^7 of **A** (a χ_1 angle of $+60°$ accounts for a P_1 conformation in a D-amino acid, whereas the P_1 conformation of a L-amino acid is represented by a χ_1 of $-60°$), one of the CH_3 groups of MeLeu^7 comes fairly close to CH_3–C(α) of Hip^2. This interaction could lead to the observed change in the ring structure. We expect a smaller distance of MeLeu^7*H*–C(β) to Hip^2*CH*$_3$–C(α) in [Me-L-Leu^7]didemnin B than in didemnin B. This assumption may be confirmed by the Hip^2*H*–C(α)/MeLeu^7*H*–C(β) NOE of **A** (see *Table 6*) which is not found in the case of didemnin B. This major difference could be responsible for the deviations in the biological activity of the two epimers.

Structure of Conformer B of [Me-L-Leu^7]Didemnin B in Solution. – The solution structure of the second most populated conformer **B** of [Me-L-Leu^7]didemnin B is not as well determined as that of conformer **A** because of the smaller number of available NOE values. The data for the NOE effects, the coupling constants, the temperature gradients, the torsion angles, and the H-bonds are given in *Tables 4–9* and will not be discussed in detail. None of the β-turns are retained in this conformer which can be realized from the *Ramachandran* plots in *Fig. 12 a–c* where the values of the dihedrals are included. The βII turn of the linear side chain involving Pro^8 in the $i + 1$ and Me-L-Leu^7 in the $i + 2$ position is converted to a βVI-turn-type structure [31] (see *Fig. 15*), which is determined by the

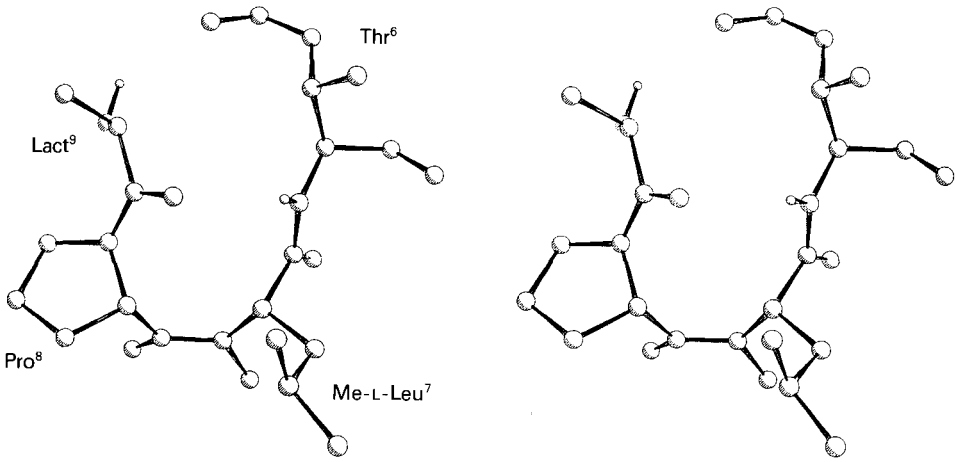

Fig. 15. *Stereoview of the βVI turn* (part of the 'mean' conformation obtained by a 50 ps restrained MD *in vacuo*) *in the linear side chain of conformer* **B** *involving Pro^8 in the* i + *1 and Me-*L*-Leu^7 in the* i + *2 position.* The *cis* peptide bond is clearly visible.

Pro^8*H*–C(α)/MeLeu^7*H*–C(α) NOE effect indicating a *cis* peptide bond. In the 'mean' conformation of the MD calculation, the *cis* peptide bond deviates by $-24°$ from planarity which may be caused by the repulsion of the MeLeu^7*CH*$_3$N group and Pro^8*CO*. A similar βVI turn determined by an *H*–C(α)/*H*–C(α) NOE was already observed for the weakly populated conformer of VDA 008, the cyclic hexapeptide cyclo(-D-Ala^1-Phe^2-Val^3-Lys(Z)^4-Trp^5-Phe^6-), involving Val^3 in the *i* position [32].

Though the MD-calculated value for the ψ angle of Me-L-Leu^7 (see *Table 8*) deviates considerably from its ideal value ($\psi = 0$) [31] in a βVI turn, this bend can be described by

a βVI turn type because of the following classification: In general, a bend belongs to the indicated turn type if the ϕ_{i+1}, ψ_{i+1}, and ϕ_{i+2} angles are within ±40° of the ideal values [33]. Those requirements are fulfilled in our case. Additionally, the βVI-turn type is indicated by the Thr^{6}NH/MeLeu^7H–C(α) NOE (254 pm).

Comparison of the Side-Chain Structure of Conformers A and B with that of Didemnin B. – The conformation of the side chains were determined as usual [34] using $^3J(H$–C(α), H–C(β)) and ^3J(H–C(α)/H′–C(β)) and COLOC cross-peak intensities. Also some NOE effects deliver the assignments of the diastereotopic β protons which is essential for the discrimination between conformation **I** ($\chi_1 = -60°$), **II** ($\chi_1 = 180°$), and **III** ($\chi_1 = +60°$). In all cases, nearly identical side-chain conformations were found in conformer **A** and didemnin B (see *Tables 5, 6,* and *9*). This supports also the above mentioned similar backbone conformation of both peptides, whereby the observed change in the ring structure (see above) is assumed to be caused by the Me-L-Leu^7 residue. Hence, its side-chain analysis will be discussed in detail.

Table 9. *MD-Calculated χ_1 Dihedrals of [Me-L-Leu^7]Didemnin B* (Conformer **A** and **B**) *in Comparison to the χ_1 Dihedrals of Didemnin B* (MD and X-ray)

Residue	[Me-L-Leu^7]Didemnin		Didemnin B	
	Conformer **A** (MD)	Conformer **B** (MD)	MD	X-ray
Ist^{1a})	84	74	64	64
Leu^3	178	55	–72	–67
Pro^4	22	26	5	36
Me$_2$Tyr^5	–65	–64	–62	–42
Thr^6	–165	–155	–153	–155
MeLeu^{7b})	–65	–117	74	61
Pro^8	–5	17	–16	–31

a) Here, the dihedral angle is N–C(γ)–C(δ)–CH$_3$.
b) Me-D-Leu^7 in the case of didemnin B.

The configuration of the residue at position 7 is L in the case of **A** and D in the case of didemnin B. As already expected, the coupling constants are reversed in the following sense: for didemnin B (Me-D-Leu^7), we observed 11.1 and 5.0 Hz for $^3J(H$–C(α), $H_{(pro\text{-}S)}$–C(β)) and $^3J(H$–C(α), $H_{(pro\text{-}R)}$–C(β)), respectively, while for **A** (Me-L-Leu^7), we find 4.9 and 10.3 Hz respectively (for the corresponding coupling constants of conformer **B**, see *Table 5*). The calculated populations [35] determine rotamer **I** or **II** in solution for **A** and **B**. The NOE between Me-D-Leu^{7}CH_3N and Me-D-Leu^7H–C(β) which was observed for didemnin B and indicated for rotamer **I** in solution was not found for the Me-L-Leu^7 derivatives **A** and **B**. But the weak COLOC correlation to one β proton of conformer **A** (see *Table 3*) and the MD-calculated χ_1 angle of –65° (**A**) and –117° (**B**) lead us to propose rotamer **I** for conformer **A** and **B** of [Me-L-Leu^7]didemnin B in solution.

In the cases where the side-chain structures of conformer **B** were accessible, the population of the rotamers are similar to those of **A**.

Conclusion. – The substitution of the Me-D-Leu residue of didemnin B by a Me-L-Leu residue induces only minor changes in the backbone conformation in the main conformation **A**. Only a slight extension of the Ist^1-Hip^2 region giving rise to a more expanded ring

is observed. On the other hand, the biological activity is considerably reduced. It is not known so far if this is due to an important contribution of the MeLeu residue in the binding or if the mentioned small backbone conformational change is sufficient to reduce the receptor binding ability of the Me-L-Leu[7] derivative in comparison to that of didemnin B.

Measurement Conditions. – *General.* All NMR spectra were recorded at 300 K on a *AM 500* spectrometer (ν_0(^{1}H) 500 MHz) equipped with an *Aspect 3000* computer *(Bruker)*. A sample containing 20 mg of material in degassed (D_6)DMSO was used for all measurements.

1. *1D ^{1}H-NMR Spectra.* Size 16 K, sweep width 5319.15, pulse length 3.0 µs, 128 acquisitions. *Lorentz* to *Gauss* multiplication ($GB = 0.3$, $LB = -3$) was applied. The spectra for determination of the temp. gradients were recorded at 300–340 K in steps of 10 K.

2. *DQF-COSY Spectrum.* Sequence: D_1-90°-t_1-90°-D_2-90°-t_2. Relaxation delay $D_1 = 1.6$ s, delay $D_2 = 4$ µs, 90°-pulse 7.7 µs, acquisition time 417.8 ms, spectral width in f_1 and f_2 4902.0 Hz, size 4 K, 32 acquisitions, 1024 increments, quadrature detection in both dimensions, single zero filling in f_1 and apodization with a squared $\pi/3$-shifted sine bell in both dimensions.

3. *NOESY Spectrum.* Sequence: D_1-90°-t_1-90°-t_1-90°-τ_{mix}-90°-t_2. Relaxation delay $D_1 = 1.5$ s, mixing time $\tau_{mix} = 120$ ms, random variation of τ_{mix} (in 10% of τ_{mix}) was applied to suppress zero quantum coherences, sweep width 5319.15 Hz in f_1 and f_2, 750 experiments in t_1, quadrature detection in both dimensions, zero filling up to 2 K in t_1 and apodization with a squared $\pi/2$-shifted sine bell in both dimensions, baseline correction. For the plot of *Fig. 9, Gauss* multiplication in both dimension was applied ($LB = -5$, $GB = 0.1$).

4. *TOCSY spectra.* Sequence: D_1-90°-t_1-MLEV17-t_2. Relaxation delay $D_1 = 1.5$ s, 90°-pulse length 10.5 µs, spectra with different mixing times (duration of the spin-lock period) were recorded: a) 20 ms b) 80 ms, sweep width 5376.34 Hz, 500 increments, size 4 K in f_2, zero filling to 1 K in f_1 and apodization with squared $\pi/3$-shifted sine bell in both dimensions.

5. *E.COSY Spectrum.* Sequence: D_1-90°-t_1-90°-D_2-90°-t_2, phase cycling for three spin E.COSY was applied in accordance to [11d], relaxation delay $D_1 = 1.4$ s, delay $D_2 = 2$ µs, 90°-pulse length 8 µs, 72 acquisitions, 940 increments, sweep width in both dimensions 3649.64 Hz, size 4 K in f_2, *Lorentz* to *Gauss* multiplication in both dimensions ($GB = 0.15$, $LB = -1.5$). For extraction of the J values, inverse *Fourier* transformation of respective rows was applied and zero filled up to 16 K.

6. *'Inverse COLOC' Spectrum.* Sequence: D_1-90°(^{1}H)-D_2-90°$_{selective}$(^{13}C)-t_1/2-180°-t_1/2-90°(^{13}C)-t_2(^{1}H). Relaxation delay 1.5 s, 90°-pulse length: 8.9 µs (^{1}H), 13.2 µs (^{13}C, hard), 2000 µs (^{13}C, soft), $D_2 = 60$ ms, sweep with in f_1 1200 Hz and in f_2 5319.15 Hz, t_1 ridges were eliminated by subtracting coadded rows of a region without cross-peaks from the 2D matrix. The spectrum was phase-sensitively recorded and processed, followed by a magnitude calculation.

7. *Proton-Detected ^{1}H,^{13}C-COSY Spectrum (HMQC).* Sequence, see *Fig. 5a.* Relaxation delay 95.1 ms, 90°-pulse length: 10.5 µs (^{1}H), 13.8 µs (^{13}C), $\Delta = 3.45$ ms, $\tau = 172.8$ ms, spectral range in f_2 5319.149 Hz and in f_1 10000 Hz (0–80 ppm), quadrature detection in both dimensions 2 dummy scans, 144 acquisitions, size 2 K, zero filling to 4 K in f_2 and to 1 K in f_1, recording and processing in the phase-sensitive mode, coadded rows of a spectral region without cross-peaks were substrated from the 2D matrix.

8. *Proton-Detected ^{1}H,^{13}C-COSY with TOCSY Transfer Spectrum.* Sequence, see *Fig. 5b.* Identical conditions as in *Exper. 8,* except that the spectral range in f_1 was expanded to 17000 Hz (0–140 ppm) and 176 acquisitions were recorded; mixing time for the spin lock, $\tau_{mix} = 80$ ms.

This work was supported by the *Deutsche Forschungsgemeinschaft* and the *Fonds der Chemischen Industrie*. We thank *P. Schmieder* and Dr. *W. Bermel (Bruker AG)* for instrumental help.

REFERENCES

[1] a) K. L. Rinehart, Jr., J. B. Gloer, R. G. Hughes, Jr., H. E. Renis, J. P. McGovren, E. B. Swynenberg, D. A. Stringfellow, S. L. Kuenzel, L. H. Li, *Science* **1981,** *212,* 933; b) K. L. Rinehart, V. Kishore, K. C. Bible, R. Sakai, D. W. Sullins, K.-W. Li, *J. Nat. Prod.* **1988,** 10; c) S. L. Crampton, E. G. Adams, S. L. Kuentzel, L. H. Li, G. Badiner, B. K. Bhuyan, *Cancer Res.* **1984,** *44,* 1796.

[2] K. L. Rinehart, V. Kishore, S. Nagarajan, R. J. Lake, J. B. Gloer, F. A. Bozich, K.-M. Li, R. E. Maleczka, Jr., W. L. Todsen, M. H. G. Munro, D. W. Sullins, R. Sakai, *J. Am. Chem. Soc.* **1987,** *109,* 6846.

[3] U. Schmidt, M. Kroner, H. Griesser, *Tetrahedron Lett.* **1988,** *29,* 3057; *ibid.* **1988,** *29,* 4407.
[4] a) Y. Hamada, Y. Kondo, M. Shibata, T. Shioivi, *J. Am. Chem. Soc.* **1989,** *111,* 669; b) W. R. Ewing, B. D. Harris, W. R. Li, M. M. Joullie, *Tetrahedron Lett.* **1989,** *30,* 3757; c) P. Jouin, J. Poncet, M. N. Dufour, A. Pantaloni, B. Castro, *J. Org. Chem.* **1989,** *54,* 617.
[5] H. Kessler, M. Will, G. M. Sheldrick, J. Antel, *Magn. Reson. Chem.* **1988,** *26,* 501.
[6] H. Kessler, M. Will, J. Antel, H. Beck, G. M. Sheldrick, *Helv. Chim. Acta* **1989,** *72,* 530.
[7] M. B. Hossain, D. van der Helm, J. Antel, G. M. Sheldrick, S. K. Sanduja, A. J. Weinheimer, *Proc. Natl. Acad. Sci. U.S.A.* **1988,** *85,* 4118.
[8] a) W. P. Aue, E. Bartholdi, R. R. Ernst, *J. Chem. Phys.* **1976,** *64,* 2229; b) U. Piantini, O. W. Sørensen, R. R. Ernst, *J. Am. Chem. Soc.* **1982,** *104,* 6800; c) M. Rance, O. W. Sørensen, G. Bodenhausen, G. Wagner, R. R. Ernst, K. Wüthrich, *Biochem. Biophys. Res. Commun.* **1983,** *117,* 479.
[9] a) L. Braunschweiler, R. R. Ernst, *J. Magn. Reson.* **1983,** *53,* 521; b) A. Bax, R. A. Byrd, A. Azalos, *J. Am. Chem. Soc.* **1985,** *106,* 7632.
[10] a) J. Jeener, B. H. Meier, P. Bachmann, R. R. Ernst, *J. Chem. Phys.* **1979,** *71,* 4546; b) K. Wüthrich, 'NMR of Proteins and Nucleic Acids', Wiley, New York, 1986.
[11] a) C. Griesinger, O. W. Sørensen, R. R. Ernst, *J. Am. Chem. Soc.* **1985,** *107,* 6394; b) *J. Chem. Phys.* **1986,** *85,* 6837; c) *J. Magn. Reson.* **1987,** *75,* 474; d) C. Griesinger, Dissertation, Frankfurt, 1986, App. B9.
[12] a) H. Kessler, W. Bermel, C. Griesinger, presented at the Sixth Meeting of the Fachgruppe Magn. Resonanzspektroskopie, Berlin, September 25–28, 1985; b) L. Lerner, A. Bax, *J. Magn. Reson.* **1986,** *69,* 375.
[13] W. Bermel, C. Griesinger, K. Wagner, *J. Magn. Reson.* **1989,** *83,* 223.
[14] H. Kessler, C. Griesinger, R. Kerssebaum, K. Wagner, R. R. Ernst, *J. Am. Chem. Soc.* **1987,** *109,* 607.
[15] H. Kessler, W. Bermel, C. Griesinger, *J. Am. Chem. Soc.* **1985,** *107,* 1083.
[16] A. Bax, M. F. Summers, *J. Am. Chem. Soc.* **1986,** *108,* 2093.
[17] A. J. Shaka, P. B. Barker, R. Freeman, *J. Magn. Reson.* **1985,** *64,* 547.
[18] A. Bax, S. Subramaniam, *J. Magn. Reson.* **1986,** *67,* 565.
[19] a) A. Bax, R. H. Griffey, B. L. Hawkins, *J. Magn. Reson.* **1983,** *55,* 81; b) L. Müller, *J. Am. Chem. Soc.* **1979,** *101,* 4481; c) M. R. Bendall, D. T. Pegg, D. M. Doddrell, *J. Magn. Reson.* **1983,** *52,* 81.
[20] H. Kessler, *Angew. Chem. Int. Ed.* **1982,** *21,* 512.
[21] H. Kessler, M. Gehrke, C. Griesinger, *Angew. Chem. Int. Ed.* **1988,** *27,* 490.
[22] H. Kessler, R. Kerssebaum, A. G. Klein, R. Obermeier, M. Will, *Liebigs Ann. Chem.* **1989,** 269.
[23] P. E. Wright, H. J. Dyson, R. A. Lerner, *Biochemistry* **1988,** *27,* 7167.
[24] H. J. Dyson, M. Rance, R. A. Houghten, R. A. Lerner, P. E. Wright, *J. Mol. Biol.* **1988,** *201,* 161.
[25] J. Aquist, W. F. van Gunsteren, M. Leijonmark, O. J. Tupia, *J. Mol. Biol.* **1985,** *183,* 461.
[26] W. F. van Gunsteren, R. Kaptein, E. R. P. Zuiderweg, 'Proceedings of the NATO/CECAM Workshop on Nucleic Acid Conformation and Dynamics', Ed. W. K. Olsen, Orsay, 1983, pp. 79–92.
[27] W. F. van Gunsteren, R. Boelens, R. Kaptein, R. M. Scheek, E. R. P. Zuiderweg, 'Molecular Dynamics and Protein Structure', Ed. J. Hermans, Polycrystal Book Service, Wester Springs, 1985, pp. 92–99.
[28] H. Kessler, J. W. Bats, C. Griesinger, S. Koll, M. Will, K. Wagner, *J. Am. Chem. Soc.* **1988,** *110,* 1033.
[29] H. J. C. Berendsen, J. P. M. Postma, W. F. van Gunsteren, A. DiNola, J. R. Haak, *J. Chem. Phys.* **1984,** *81,* 3684.
[30] K. Wagner, Dissertation, Frankfurt, 1988.
[31] G. D. Rose, L. M. Gierasch, J. A. Smith, *Adv. Protein Chem.* **1985,** *37,* 1.
[32] U. Anders, Dissertation, Frankfurt, 1989, pp. 98.
[33] a) G. Némethy, H. A. Scheraga, *Biochem. Biophys. Res. Commun.* **1980,** *95,* 320; b) S. S. Zimmerman, H. A. Scheraga, *Biopolymers* **1977,** *16,* 811.
[34] H. Kessler, C. Griesinger, K. Wagner, *J. Am. Chem. Soc.* **1987,** *109,* 6927.
[35] a) K. G. R. Pachler, *Spectrochim. Acta* **1963,** *19,* 2085; b) *ibid.* **1964,** *20,* 581; c) V. F. Bystrov, Prog. *Nucl. Magn. Reson. Spectrosc.* **1976,** *10,* 41.